IJRCS

International Journal of Robotics and Control Systems
Vol. 4, No. 1, 2024, pp. 50-68
ISSN 2775-2658
http://pubs2.ascee.org/index.php/ijrcs

ASCEE

Induction Motor Performance Improvement using Super Twisting SMC and Twelve Sector DTC

Yassine Zahraoui [a,1,*], Mohamed Moutchou [a,2], Souad Tayane [a,3], Chaymae Fahassa [b,4], Sara Elbadaoui [b,5]

[a] CCPS Lab, Higher National School of Arts and Crafts, Hassan II University, Casablanca 20670, Morocco
[b] PEC Lab, Mohammadia School of Engineers, Mohammed V University, Rabat 10090, Morocco
[1] yassine.zahraoui1-etu@etu.univh2c.ma; [2] mohamed.moutchou@univh2c.ma; [3] souad.tayane@univh2c.ma;
[4] fahassa.chaymae@gmail.com; [5] sara_elbadaoui@um5.ac.ma
[*] Corresponding Author

ARTICLE INFO

Article History
Received June 27, 2023
Revised July 13, 2023
Accepted January 15, 2024

Keywords
Induction Motor;
Performance Improvement;
Integral Super Twisting Smc;
Twelve Sector DTC;
Fuzzy Luenberger Observer;
Ripple Reduction

ABSTRACT

Induction motor (IM) direct torque control (DTC) is prone to a number of weaknesses, including uncertainty, external disturbances, and non-linear dynamics. Hysteresis controllers are used in the inner loops of this control method, whereas traditional proportional-integral (PI) controllers are used in the outer loop. A high-performance torque and speed system is consequently needed to assure a stable and reliable command that can tolerate such unsettled effects. This paper treats the design of a robust sensorless twelve-sector DTC of a three-phase IM. The speed controller is conceived based on high-order super-twisting sliding mode control with integral action (iSTSMC). The goal is to decrease the flux, torque, the current ripples that constitute the major conventional DTC drawbacks. The phase current ripples have been effectively reduced from 76.92% to 45.30% with a difference of 31.62%. A robust adaptive flux and speed observer-based fuzzy logic mechanism are inserted to get rid of the mechanical sensor. Satisfactory results have been got through simulations in *MATLAB/Simulink* under load disturbance. In comparison to a conventional six-sector DTC, the suggested technique has a higher performance and lower distortion rate.

1. Introduction

The induction motor (IM) (also called an asynchronous motor) is the most used motor in the industry. It is reliable, efficient, robust, and low-cost compared to other motors (DC-motors and PMSMs) for analogous applications [1]. However, its precise control is complicated to achieve due to its non-linear structure, its dynamics, and the variation of its internal parameters during its running and it is subject to unrecognized disturbances such the load torque; furthermore, some of its states are not reachable by a measurement [2].

During the last two decades, a very appreciable development towards the control of the induction motor has been noted, such as the vector control by flux orientation [3], the non-linear control [4], the control by sliding mode [5], the control by linearisation inputs/outputs [6] ...etc., as well as DTC [7]. This last constituent is the research heart of this scientific paper.

DTC was formulated by *Takahashi* in the mid-1980s. It is established on a control sequence

direct application to the inverter voltage switches positioned upstream of the induction motor [8]. This sequence choice is done by a switching table usage and 2 hysteresis regulators whose job is to command the motor stator flux and electromagnetic torque [9].

This control quickly gave satisfaction, and its success made it more and more popular. It is a subject of interest for many scientists and industrialists in the field of variable speed applications such as electric traction (metro and high-speed trains *TGV*), aerospace, or in certain electric car prototypes [10]. However, experience has shown some weaknesses of this type of control such as the performance at the variable switching frequency, the existence of torque pulsations, and the method of obtaining the estimated flux in the DTC which is based on straight measurement of voltage and current instantaneous values. This kind of estimator is sensitive to integration errors at low speed and can lead to considerable estimation errors. Also, the closed-loop speed regulation in the DTC is usually done by a simple PI controller [11]. Although these regulators are exceptionally successful on the market, the fact remains that the determination of their parameters (*Proportional* and *integral* gains) sometimes remains difficult when the controlled system is prone to exterior disturbances (they are not equipped with a disturbance estimator) [12].

The first-order SMCs generalization yields higher-order SMCs. This method, which uses higher-order derivatives rather than just a sliding surface first derivative to achieve exceptional durability and minimized chattering, makes it practical for electric drives [13]. Notably for systems where the command rule occurs in the sliding variable first derivative, the sliding mode super twisting control (SMC-ST) method has lately gained a lot of interest [14].

The gathering of speed data is an essential part of DTC for controlling the induction motors torque and speed. In order to generate the reference torque, speed is often monitored using mechanical sensors and afterward fed back into the inner loops. Several methods have been developed to solve this issue, inclosing open-loop estimators [15], full-order observers [16], reduced-order observers [17], model reference adaptive systems [18], Kalman filters [19], and neural networks [20]. Mechanical sensors experience tear and wear over time as they are continuously employed.

A technique known as the adaptive Luenberger observer (ALO) is an appealing performance-enhancing option for sensorless schemes because of its prompt response time and dynamic robustness versus noise, faulty parameters, and external disturbances. The use of adaptive observers (AOs) for sensorless motor drive control has already been suggested in the literature. Considering these limitations, it can be very difficult to increase the observers robustness by simultaneously calculating the rotor flux, speed, and machine parameters. By carefully choosing the observer feedback matrix gains, it is feasible to increase resilience even in the presence of parameter variation [21].

This research purpose is to enhance the operation of the DTC applied to the IM drive. We propose a robust DTC strategy based on high-order sliding mode regulators with integral action (also called super twisting), in order to command the switching table allowing the best choice of the vector voltage sequence to be delivered to the machine while observing the torque and flux constraints [22]. The aim of this command is to enhance the speed response and to decrease the ripple level. In the end, sliding mode theory is more stable and resistant to disturbances than PI control, and its implementation in software and hardware is very quite simple [23].

This research aims to enhance the classical DTC performance by substituting the PI controller with a robust one. The suggested speed controller is obtained by analyzing the induction motor equivalent model impact on the speed control:

- Planning a robust speed regulator based on the high-order sliding mode theory.
- Improving the sensorless operation by inserting a robust fuzzy adaptive observer.

This paper is structured as: Section 1 introduces the topic and the literature review. Section 2 details the induction motor mathematical model. Section 3 discusses the conventional and the sug-

gested DTC fundamentals. Section 4 illustrates the suggested iSTSMC controller. Section 5 explains the fuzzy adaptive observer. Section 6 presents the simulation environment and the discussion of the results. At last, section 7 concludes the paper.

2. Induction Motor Mathematical Modeling

The induction motor state representation depends on the selected frame and the state variables choice for the electrical equations. The state variables choice bases on the objectives, command task, or observation. The following equation system describes the induction motor mathematical model:

$$\begin{cases} \dot{X} = A_1 X + B_1 U \\ Y = C_1 X \end{cases} \tag{1}$$

The state vector is X=$[I_{s\alpha}\ I_{s\beta}\ \Phi_{r\alpha}\ \Phi_{r\beta}]^t$, the input vector is U=$[V_{s\alpha}\ V_{s\beta}]^t$, and the output vector is Y=$[I_{s\alpha}\ I_{s\beta}]^t$. The stator currents $I_{s\alpha}$, $I_{s\beta}$ and the rotor fluxes $\Phi_{r\alpha}$, $\Phi_{r\beta}$ are the state and the input vectors components. The stator voltages $V_{s\alpha}$ and $V_{s\beta}$ constitute the output vector.

This choice of variable is justified on the one hand, by the fact that the stator currents are measurable and on the other side because the norm of the rotor flux must be commanded. All these quantities are expressed on their stationary reference frame α-β to be easily manipulated by the DTC control [24]. The control matrix is A_1, the input matrix is B_1, and the output matrix is C_1. They are defined as:

$$A_1 = \begin{bmatrix} -a_1 & 0 & \frac{a_2}{\tau_r} & a_2\Omega_r \\ 0 & -a_1 & -a_2\Omega_r & \frac{a_2}{\tau_r} \\ \frac{M}{\tau_r} & 0 & -\frac{1}{\tau_r} & -\Omega_r \\ 0 & \frac{M}{\tau_r} & \Omega_r & -\frac{1}{\tau_r} \end{bmatrix}; B_1 = \begin{bmatrix} \frac{1}{bL_s} & 0 \\ 0 & \frac{1}{bL_s} \\ 0 & 0 \\ 0 & 0 \end{bmatrix}; C_1 = \begin{bmatrix} 1 & 0 & 0 & 0 \\ 0 & 1 & 0 & 0 \end{bmatrix}$$

with a_1=$\frac{R_s}{bL_s}$+$\frac{1-b}{bT_r}$; a_2=$\frac{1-b}{bL_m}$; b=1-$\frac{L_m^2}{L_s L_r}$; τ_r=$\frac{L_r}{R_r}$, and b is the Blondel's coefficient. As the electromechanical power is:

$$P_{em} = p\frac{M}{L_r}(\Phi_{r\alpha} I_{s\beta} - \Phi_{r\beta} I_{s\alpha})\Omega_r \tag{2}$$

By dividing P_e by the mechanical speed Ω_r, the electromagnetic torque can be then calculated easily:

$$T_{em} = p\frac{M}{L_r}(\Phi_{r\alpha} I_{s\beta} - \Phi_{r\beta} I_{s\alpha}) \tag{3}$$

The rotor speed is described as:

$$J\frac{d\Omega_r}{dt} = T_{em} - T_l - f\Omega_r \tag{4}$$

where J is the inertia of the motor, T_l is the torque of the load, and f is the coefficient of friction. Fig. 1 demonstrates the induction motor matrix model.

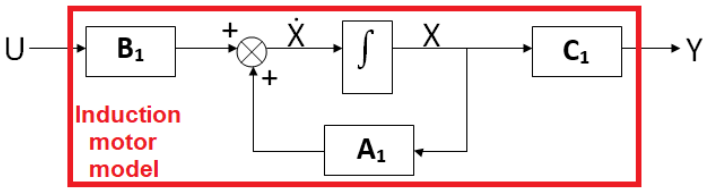

Fig. 1. Induction motor state-space matrix model

3. DTC Fundamentals

By choosing the best inverter switching states, DTC's main goal is to directly and separately command the flux and the torque inside their hysteresis bounds. DTC offers outstanding torque command operation, particularly in terms of a quick response, and does not need coordinate transformation, current controllers, or PWM block [25].

3.1. Flux and Torque Estimation

Basing on the stator voltages and currents measurements, the torque and the flux can be estimated. The flux can be formulated using the IM dynamics in the fixed reference:

$$\Phi_s = \int_0^t (V_s - R_s I_s) dt \tag{5}$$

as a result, the α-β flux components are:

$$\begin{cases} \Phi_{s\alpha} = \int_0^t (V_{s\alpha} - R_s I_{s\alpha}) dt \\ \Phi_{s\beta} = \int_0^t (V_{s\beta} - R_s I_{s\beta}) dt \end{cases} \tag{6}$$

Based on the stator flux components in the α-β reference, the flux module can be determined, which may be theoretically defined as:

$$\Phi_s = \sqrt{\Phi_{s\alpha}^2 + \Phi_{s\beta}^2} \tag{7}$$

The product difference between the stator current and the stator flux in different references can be used to define the electromagnetic torque, as shown in the equation (8) below:

$$T_{em} = p(I_{s\beta}\Phi_{s\alpha} - I_{s\alpha}\Phi_{s\beta}) \tag{8}$$

3.2. Conventional DTC Switching Table

Errors caused by the discrepancy between reference and estimated values are inputs to the hysteresis comparators. The switching table's input selection is in the meantime determined by the hysteresis controllers outputs and flux locations. The appropriate switching state vector is then selected by the selector. The classical DTC switching table is shown in Table 1.

Table 1. The conventional DTC switching table

$\Delta\Phi_s$	ΔT_{em}	S_1	S_2	S_3	S_4	S_5	S_6
1	1	110	010	011	001	101	100
	0	111	000	111	000	111	000
	-1	101	100	110	010	011	001
0	1	010	011	001	101	100	110
	0	000	111	000	111	000	111
	-1	001	101	100	110	010	011

Eight position vectors ($\vec{V}_1$, $\vec{V}_2$, . . ., $\vec{V}_8$) are produced by this switching look-up table (S_a S_b S_c), 2 of them are null (S_a S_b S_c)=(1 1 1) or (0 0 0).

3.3. Performance Improvement Basing on Twelve Sector Partition

The estimated torque and flux are compared to their references. The comparison results is the hysteresis controllers inputs. The flux is regulated using a 3-level comparator, while the torque is regulated using a 5-level comparator, as shown in Fig. 2.

The flux locus is divided into twelve sectors of 30° each. Two switching states per sector, $\vec{V}_i$ and $\vec{V}_{i+3}$, are not taken into account in the conventional six sector DTC. As a result, the torque control is

not efficient at its best. A zone shifting considers the first sector from $\frac{11\pi}{6}$ to $\frac{\pi}{6}$ rather than taking it from 0 to $\frac{\pi}{3}$. A new switching table can be then created. Additionally, this new partition contains 2 unused vectors per sector ($\vec{V}_{i+2}$ and $\vec{V}_{i-1}$), which ambiguously affects the flux control as opposed to the torque. So, a different method was created that, as shown in Fig. 3, divides the flux locus into 12 sectors instead of the conventional 6 sectors [26].

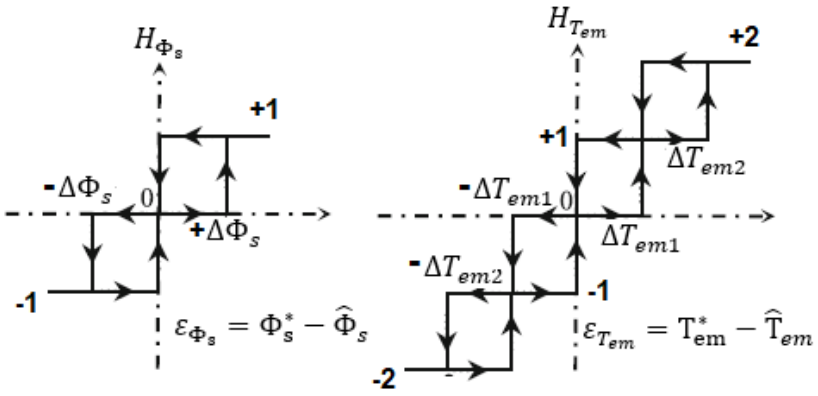

Fig. 2. Torque and flux hysteresis controllers

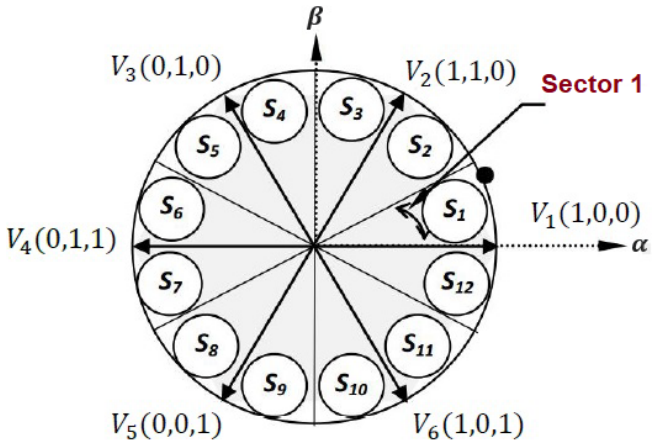

Fig. 3. Voltage vector in 12 sectors partition

As consequence, each sector will use all 6 states and ambiguity in flux and torque command can be avoided. The vector $\vec{V}_1$ causes a significant increase in flux and a minor increase in torque in the twelve DTC. In contrast, $\vec{V}_2$ causes a significant increase in torque and a negligible rise in flux. Consequently, it is necessary now to define the variations of small and large torque [27]. This idea results in a four-part division of the torque's hysteresis band. Table 2 below offers then the twelve sector switching table.

According to several research, adding more sectors marginally reduced high ripples and current harmonics [28], [29], [30]. Space vector modulation (SVM) also offers well dynamics in the low and high-speed range [31].

4. Integral Sliding Mode Super-Twisting Control

4.1. Principle

A novel strategy for enhancing integral sliding mode control (iSMC) operation, typically, for rejecting disturbance and reducing chattering by fusing iSMC with super-twisting (ST) control, is

Table 2. Twelve sector DTC – the suggested switching table

$\Delta\Phi_s$	ΔT_{em}	S_1	S_2	S_3	S_4	S_5	S_6	S_7	S_8	S_9	S_{10}	S_{11}	S_{12}
	2	V_{21}	V_{16}	V_{22}	V_{17}	V_{23}	V_{18}	V_{24}	V_{19}	V_{25}	V_{20}	V_{26}	V_{15}
	1	V_{21}	V_2	V_{22}	V_3	V_{23}	V_4	V_{24}	V_5	V_{25}	V_6	V_{26}	V_1
1	0	V_0	V_7	V_{14}	V_0	V_7	V_{14}	V_0	V_7	V_{14}	V_0	V_7	V_{14}
	-1	V_{26}	V_1	V_{21}	V_2	V_{22}	V_3	V_{23}	V_4	V_{24}	V_5	V_{25}	V_6
	-2	V_{26}	V_{15}	V_{21}	V_{16}	V_{22}	V_{17}	V_{23}	V_{18}	V_{24}	V_{19}	V_{25}	V_{20}
	2	V_{22}	V_{17}	V_{23}	V_{18}	V_{24}	V_{19}	V_{25}	V_{20}	V_{26}	V_{15}	V_{21}	V_{16}
	1	V_{22}	V_3	V_{23}	V_4	V_{24}	V_5	V_{25}	V_6	V_{26}	V_1	V_{21}	V_2
0	0	V_0	V_7	V_{14}	V_0	V_7	V_{14}	V_0	V_7	V_{14}	V_0	V_7	V_{14}
	-1	V_{25}	V_6	V_{26}	V_1	V_{21}	V_2	V_{22}	V_3	V_{23}	V_4	V_{24}	V_5
	-2	V_{25}	V_{20}	V_{26}	V_{15}	V_{21}	V_{16}	V_{22}	V_{17}	V_{23}	V_{18}	V_{24}	V_{19}
	2	V_{17}	V_{23}	V_{18}	V_{24}	V_{19}	V_{25}	V_{20}	V_{26}	V_{15}	V_{21}	V_{16}	V_{22}
	1	V_3	V_{23}	V_4	V_{24}	V_5	V_{25}	V_6	V_{26}	V_1	V_{21}	V_2	V_{22}
-1	0	V_0	V_7	V_{14}	V_0	V_7	V_{14}	V_0	V_7	V_{14}	V_0	V_7	V_{14}
	-1	V_5	V_{25}	V_6	V_{26}	V_1	V_{21}	V_2	V_{22}	V_3	V_{23}	V_4	V_{24}
	-2	V_{19}	V_{25}	V_{20}	V_{26}	V_{15}	V_{21}	V_{16}	V_{22}	V_{17}	V_{23}	V_{18}	V_{24}

suggested in this research. A new integral sliding mode super-twisting control (iSTSMC) law can be created by combining the iSMC equivalent control part and the ST discontinuous control part [32], [33]:

$$T_{em}^{*} = T_{em_{eq}} + T_{em_{ST}} \tag{9}$$

Basing on the iSMC theory, a new surface is chosen:

$$S(t) = e(t) - \int_0^t \gamma e(\tau) d\tau \tag{10}$$

where $T_{em_{eq}}$ is defined as:

$$\begin{cases} T_{em_{ST}} = J[-\alpha_\Omega \sqrt{|(S(t))|} sign(S(t)) + T_{em_1}] \\ \dot{T}_{em_1} = -\beta_\Omega sign(S(t)) \end{cases} \tag{11}$$

whence,

$$T_{em_{ST}} = J[-\alpha_\Omega \sqrt{|(S(t))|} sign(S(t)) - \beta_\Omega \int_0^t sign(S(\tau) d\tau)] \tag{12}$$

The two gains α_Ω and β_Ω are determined as:

$$\begin{cases} \beta_\Omega > \frac{\eta}{\delta_M} \\ \alpha_\Omega \geqslant \frac{4\eta\delta_M(\beta_\Omega+\eta)}{\delta_m^3(\beta_\Omega-\eta)} \end{cases} \tag{13}$$

where η designates the uncertain function Φ lower and upper positive bands at the sliding manifold second derivative, which in this instance is Ω_r, and δ_M and δ_m represent the uncertain function μ lower and upper positive bands, respectively.

$$\eta \geqslant \Phi \ \ and \ \ \delta_M \geqslant \mu \geqslant \delta_m \tag{14}$$

$$\hat{\dot{\Omega}}_r = \Phi(x,t) + \mu(x,t)\dot{T}_{em} \tag{15}$$

η, δ_M and δ_m are regarded as positive constants in this equation. As a result, the suggested control law employing the sliding surface presented in (10) can be structured as follows:

$$\begin{aligned} T_{em_{ST}}^{*} =& J[\frac{f}{J}\Omega_r + f + \dot{\Omega}_r^{*}(t) + \gamma e(t)] + \\ & J[-\alpha_\Omega \sqrt{|(S(t))|} sign(S(t)) - \beta_\Omega \int_0^t sign(S(\tau) d\tau)] \end{aligned} \tag{16}$$

4.2. Stability Analysis for Integral Super-twisting SMC

The Lyapunov-based stability of the suggested command law is thus covered in the next part. The iSTSMC-based law should satisfy the Lyapunov stability. Here, the closed-loop system stability is demonstrated using a common STC technique [34] [35]. A new space vector is also given as:

$$\begin{cases} Z_{ST} = (z_1, z_2)^t = (\lambda_\omega \sqrt{|(S(t))|} sgn(S(t)), u_1) \\ \dot{u}_1 = -\beta_\omega sgn(S(t)) \end{cases} \tag{17}$$

A function of Lyapunov stability To demonstrate the suggested regulator stability, V_{iSTC} is chosen:

$$V_{iST} = \frac{1}{2} z_{ST}^t Q z_{ST} \tag{18}$$

Q is a positive matrix with the following definition:

$$Q = \begin{bmatrix} q_{11} & q_{12} \\ q_{21} & q_{22} \end{bmatrix} \tag{19}$$

The derivative of (18) can be expressed as follows:

$$\dot{V}_{iST} = z_{ST}^t Q \dot{z}_{ST} \leqslant 0 \tag{20}$$

A quadratic Lyapunov equation's answer is as follows:

$$A^t Q + QA = -P \tag{21}$$

where P=PT>0, A is Hurwitz given as:

$$A = \begin{bmatrix} -\frac{1}{2}\alpha_\omega & \frac{1}{2} \\ -\beta_\omega & 0 \end{bmatrix} \tag{22}$$

Therefore, $\dot{V}_{iSTC}$ in (20) can be represented as follows by applying the solution in (21) and replacing z_{ST} into (19):

$$\begin{cases} \dot{V}_{iSTC} = \frac{-1}{\sqrt{|S(t)|}} z_{ST}^t [-A^t Q - QA] \dot{z}_{ST} \\ \dot{V}_{iSTC} = \xi_{min} [-A^t Q - QA] \frac{1}{\sqrt{\xi_{min}}} Q || Z_{ST}^t || \leqslant 0 \end{cases} \tag{23}$$

Where $\frac{1}{\sqrt{|S(t)|}} \neq 0$. By resolving the linear matrix inequality (LMI), the matrix $A^t Q$+QA can be made to be negative:

$$A^t Q + QA < 0 \tag{24}$$

The proposed control paradigm now possesses a stable state.

5. Adaptive Luenberger Observer

5.1. Principle

The Luenberger observer is generally described by the following state equation:

$$\begin{cases} \dot{\hat{X}} = A_{\Omega_r} \hat{X} + B_1 U + L_1 (Y - \hat{Y}) \\ Y = C_1 \hat{X} \end{cases} \tag{25}$$

The purpose of this observer is to make the observed state converge toward its real value [36]. The observer margin can be given as:

$$\varepsilon = X - \hat{X} \tag{26}$$

The observer error dynamics can also be defined as a function of the gain matrix L_1:

$$\dot{\varepsilon} = (A_{\Omega_r} - L_1 C_1)\varepsilon \tag{27}$$

The observer dynamics are given by the following characteristic equation:

$$det(sI - (A_{\Omega_r} - L_1 C_1)) = 0 \tag{28}$$

The observer matrix L_1 gains are selected by the classical pole placement method. The common rule is to select the observer poles 5 to 6 times quicker than those of the observed system.

5.2. Application to Induction Motor Flux and Speed Observation

The matrix $\hat{A}_{\Omega_r}$ is an estimate of the matrix A_{Ω_r} when the mechanical speed is a parameter to be observed and L_1 denotes the matrix of the gains of the observer:

$A_{\Omega_r}=\begin{bmatrix} -\lambda I_2 & \gamma(\frac{I_2}{\tau_r} - \hat{\Omega}_r J) \\ \frac{M}{\tau_r} I_2 & -(\frac{I_2}{\tau_r} - \hat{\Omega}_r J) \end{bmatrix}$; $L_1=-\begin{bmatrix} l_1 I_2 & l_2 J \\ l_3 I_2 & l_4 J \end{bmatrix}=\begin{bmatrix} L_1' \\ L_2' \end{bmatrix}$

In equation (25), the observed state variables are $\hat{X}=\begin{bmatrix} \hat{Y}_s & \hat{\Phi}_r \end{bmatrix}^t$. The observer gain matrix is multiplied by the error vector ε_{I_s}=I_s-$\hat{I}_s$, where I_s and $\hat{I}_s$ are the real and observed stator current vectors respectively. The observed mechanical speed is generated from an adaptation mechanism.

The observer gain matrix L_1 must provide stability and observational dynamics such that A_{Ω_r}-L_1C_1 is asymptotically stable. Thus, this matrix should be chosen such that all eigenvalues of A_{Ω_r}-L_1C_1 have negative real parts.

To guarantee the entire speed range stability, the classic procedure consists in choosing the observer poles proportional to the motor poles. Let's define k, the unique adjustment proportionality constant of generally small value ($k \geqslant 1$) [37].

If the induction motor poles are given by p_{IM}, the observer poles p_{LO} are selected by the following expression:

$$p_{LO} = k \times p_{IM} \tag{29}$$

The open loop system characteristic equation $det[p_{IM} I_2$-$A_{\Omega_r}]$=0 is defined as:

$$p_{IM}^2 + (\lambda I_2 + \frac{I_2}{\tau_r} - \Omega_r J)p_{IM} + (\alpha I_2 - \gamma \frac{M}{\tau_r} I_2)(\frac{I_2}{\tau_r} - \Omega_r J) = 0 \tag{30}$$

The observer dynamics is specified in closed loop according to the next characteristic equation $det[p_{LO} I_2 - (A_{\Omega_r} - L_1 C_1)]$=0:

$$p_{LO}^2 + (L_1 + \lambda I_2 + \frac{I_2}{\tau_r} - \Omega_r J)p_{LO} + [(\lambda I_2 - \alpha \frac{M}{\tau_r} I_2) - (L_1 + \alpha L_2)](\frac{I_2}{\tau_r} - \Omega_r J) = 0 \tag{31}$$

By substituting (29) in (31) and by identifying $k^2 \times$ (30) and (31), the observer gain matrix coefficients are:

$$\begin{cases} l_1 = (k-1)(\lambda + \frac{1}{\tau_r}) \\ l_2 = -(k-1)\hat{\Omega}_r \\ l_3 = (k^2-1)(\frac{\lambda}{\gamma} - \frac{M}{\tau_r}) + \frac{k-1}{\gamma}(\alpha + \frac{1}{\tau_r}) \\ l_4 = -\frac{(k-1)}{\gamma}\hat{\Omega}_r \end{cases} \tag{32}$$

The adaptation mechanism is deduced from Lyapunov's theorem. The observation margin on the rotor flux and the stator current, that is none other than the margin between the observer and the motor model, is expressed by:

$$\dot{\varepsilon} = (A_{\Omega_r} - L_1 C_1)\varepsilon - \Delta A_{\Omega_r} \hat{x} \tag{33}$$

The state error matrix ΔA_{Ω_r} is expressed by:

$$\Delta A_{\Omega_r} = A_{\Omega_r} - \hat{A}_{\Omega_r} = \begin{bmatrix} 0 & \gamma\Delta\Omega_r J \\ 0 & -\Delta\Omega_r J \end{bmatrix} \tag{34}$$

The variation ΔA_{Ω_r} becomes zero when Ω_r is measured. When it is not, it is assumed as an unknown constant parameter where ε=X-$\hat{X}$=$[\varepsilon_{I_{s\alpha}} \varepsilon_{I_{s\alpha}} \varepsilon_{\Phi_{r\alpha}} \varepsilon_{\Phi_{r\beta}}]^t$ and $\Delta\Omega_r$=Ω_r-$\hat{\Omega}_r$.

5.3. Stability Analysis of Adaptive Luenberger Observer

Let Lyapunov's candidate positive function be defined by:

$$V = \varepsilon^t \varepsilon + \frac{(\Delta\Omega_r)^2}{\chi} \tag{35}$$

Its time derivative is:

$$\dot{V} = \dot{\varepsilon}^t \varepsilon + \varepsilon^t \dot{\varepsilon} + \frac{2}{\chi}\Delta\Omega_r \hat{\Omega}_r \tag{36}$$

By replacing $\dot{\varepsilon}$ by its expression given in (35), (36) becomes:

$$\dot{V} = \varepsilon^t[(A_{\Omega_r} - L_1 C_1)^t + (A_{\Omega_r} - L_1 C_1)]\varepsilon - 2\mu(\varepsilon_{I_{s\alpha}} \hat{\Phi}_{r\beta} - \varepsilon_{I_{s\beta}} \hat{\Phi}_{r\alpha})\Delta\Omega_r + \frac{2}{\chi}\Delta\Omega_r \hat{\Omega}_r \tag{37}$$

With $\varepsilon_{I_{s\alpha}}$=$I_{s\alpha}$-$\hat{I}_{s\alpha}$ et $\varepsilon_{I_{s\beta}}$=$I_{s\beta}$-$\hat{I}_{s\beta}$. A sufficient condition to have an asymptotic stability is that it is necessary to cancel the last two terms of (37) so that $\dot{V}$ is negative, since the other terms of the second member of this equation are always negative, the observer rotor speed adaptation law is then deduced by:

$$\hat{\Omega}_r = \chi\mu \int_0^t (\varepsilon_{i_{s\alpha}} \hat{\phi}_{r\beta} - \varepsilon_{i_{s\beta}} \hat{\phi}_{r\alpha}) dt \tag{38}$$

Where χ is given as a positive parameter. Nevertheless, this adaptation law has been applied for an almost constant speed. To enhance the dynamics of observation of the speed, it is generally proposed to use a PI regulator instead of a pure integrator [38], and (38) can be written as:

$$\hat{\Omega}_r = K_p(\varepsilon_{I_{s\alpha}} \hat{\Phi}_{r\beta} - \varepsilon_{I_{s\beta}} \hat{\Phi}_{r\alpha}) + K_i \int_0^t (\varepsilon_{I_{s\alpha}} \hat{\Phi}_{r\beta} - \varepsilon_{I_{s\beta}} \hat{\Phi}_{r\alpha}) dt \tag{39}$$

With K_p and K_i are the PI regulator gains.

5.4. Fuzzy Logic Approach of Luenberger Observer

The rotational speed estimation techniques basing on the induction motor model have the disadvantage of dependence on the motor parameters which adds to the difficulties of adjusting the gains of the adaptation mechanism. In this paragraph, a fuzzy adaptation mechanism will be proposed to observe the induction motor rotational speed. Thus, the error ε_Ω will be adjusted using a fuzzy controller (FLC) replacing the classic PI regulator. The error ε_Ω=$\varepsilon_{I_{s\alpha}} \hat{\Phi}_{r\beta}$-$\varepsilon_{I_{s\beta}} \hat{\Phi}_{r\alpha}$ and the variation of the error $\Delta\varepsilon_\Omega$=ε_{Ω_k}-$\varepsilon_{\Omega_{k-1}}$ are then regarded as the fuzzy controller input variables, whose fuzzy output will give the estimated speed variation $\Delta\hat{\Omega}_r$=$\hat{\Omega}_k$-$\hat{\Omega}_{k-1}$ [39]. Fig. 4 shows the adaptation mechanism fuzzy regulator structure.

The estimated input and output linguistic variables*fuzzification* was reached by symmetric triangular membership functions on a normalized speech universe on the interval [-1,+1] for each variable as illustrated in Fig. 5 [40].

Furthermore, the inference rules utilized to establish the output variable as a function of the input variables are gathered in Table 3 above.

Table 3. The fuzzy mechanism inference matrix

$\Delta\varepsilon_{\Omega_n}\vert\varepsilon_{\Omega_n}$	NB	NM	NS	Z	PS	PM	PB
PB	Z	PS	PM	PB	PB	PB	PB
PM	NS	Z	PS	PM	PB	PB	PB
PS	NM	NS	Z	PS	PM	PB	PB
Z	NB	NM	NS	Z	PS	PM	PB
NS	NB	NB	NM	NS	Z	PS	PM
NM	NB	NB	NB	NM	NS	Z	PS
NB	NB	NB	NB	NB	NM	NS	Z

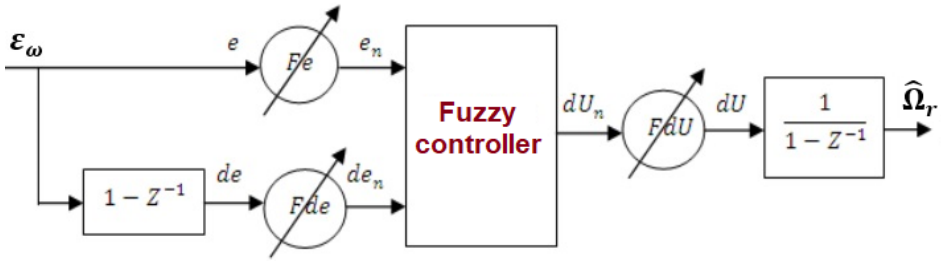

Fig. 4. The observer fuzzy mechanism block diagram

N is Negative, P is Positive, B is Big, M is Medium, S is Small, and Z is Zero. NB hence means Negative Big. The triangular membership functions in fuzzy control drive to a good linguistic classification which has positive effects on control and operational decisions. Fig. 6 shows the suggested control schema.

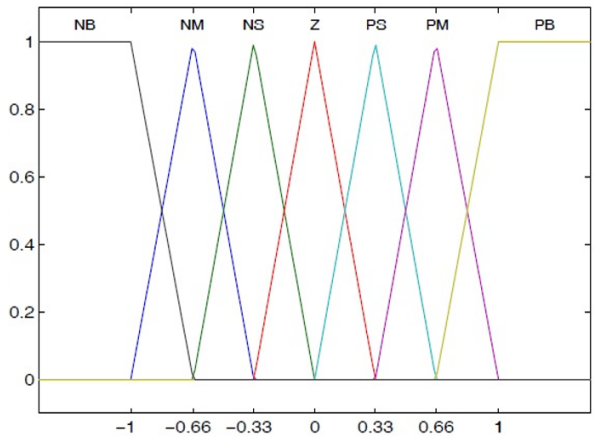

Fig. 5. Membership functions of the observer fuzzy mechanism

6. Results and Discussion

6.1. Simulation Environment

A full comparison of the conventional DTC and the suggested 12-sector iSTSMC-DTC-based fuzzy ALO is presented in this research paper. The simulation results have been got by the famous simulation software *MATLAB/Simulink*. The rated parameters and power of the motor used in the simulation are listed in Table 4.

The tests in Fig. 7 and Fig. 11 highlight the induction machine starting according to a ramp speed of 100 *rad/s*. A load of 10 *N.m* is applied at t_1=0.8*s* and removed at t_2=1.8*s* to prove the system's robustness.

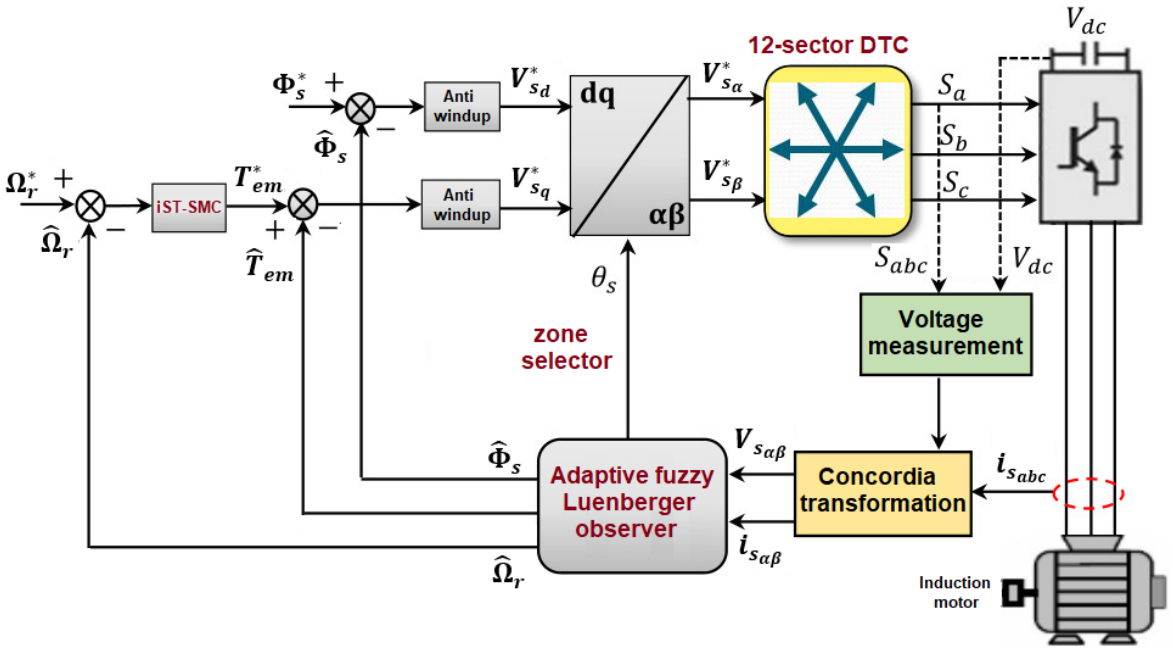

Fig. 6. The suggested control schema

Table 4. Parameters of the induction motor used in the simulation

Rated power	**3** kW
Rated speed	**1440** rpm
Pair pole	2
Frequency	50 Hz
Line voltage	220 / 380 V
Phase current	12.5 / 7.2 A
Stator resistance	2.2 Ω
Rotor resistance	2.68 Ω
Stator inductance	0.229 H
Rotor inductance	0.229 H
Mutual inductance	0.217 H
Moment of inertia	0.047 $kg.m^2$
Viscous friction coefficient	0.004 $N.s.rad^{-1}$

6.2. Results Discussion

We can clearly see that both techniques have good dynamics when starting up. The applied load disturbance does not assign the speed track a lot. The proposed iSTSMC-DTC in Fig. 7(b) maintains a good speed response better than the classical DTC in Fig. 7(a). The proposed technique is more robust, and the speed error in Fig. 7(d) is lower than that of the conventional technique in Fig. 7(c).

As mentioned before, a load of 10 *N.m* is applied at 0.8*s* and removed at 1.8*s*. The electromagnetic torque waveform of the suggested technique in Fig. 7(f) is smoother than that of the conventional DTC in Fig. 7(e), the smoothest the torque is, the lowest the THD is. This is well shown in Fig. 8(b) when the proposed technique has a reduced ripple level (54.89%) compared to conventional DTC (88.72%) in Fig. 8(a).

Both the basic DTC and the suggested iSTSMC-DTC show stable waveforms in their flux responses. The stator flux tracks perfectly its reference which is 1 *Wb*. Nevertheless, the basic DTC in Fig. 7(g) shows a chopped stator flux waveform which indicates a high ripple level, while the proposed DTC in Fig. 7(h) shows a smoother waveform. This is justified in Fig. 9(b) where the suggested iSTSMC-DTC has a lower THD level (71.97%) compared to the basic DTC (119.73%) in Fig. 9(a).

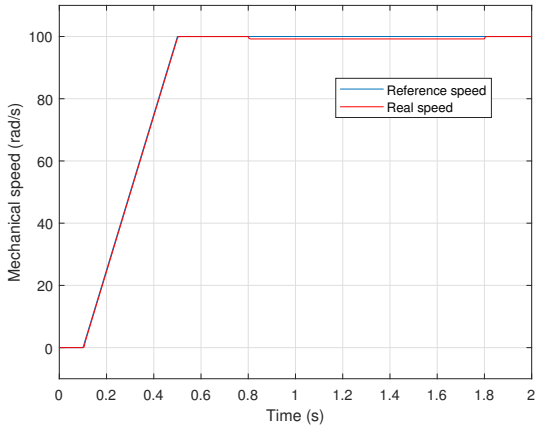

(a) Mechanical speed: conventional DTC

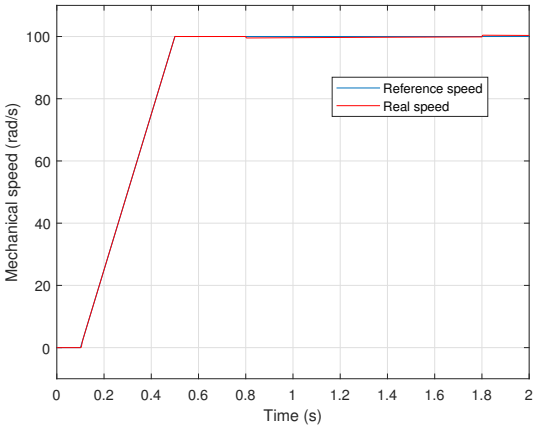

(b) Mechanical speed: proposed DTC

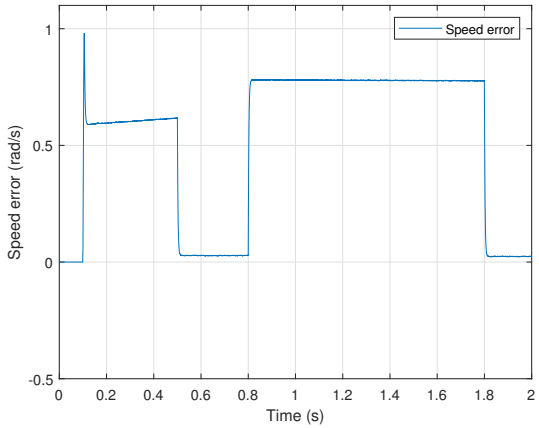

(c) Speed error: conventional DTC

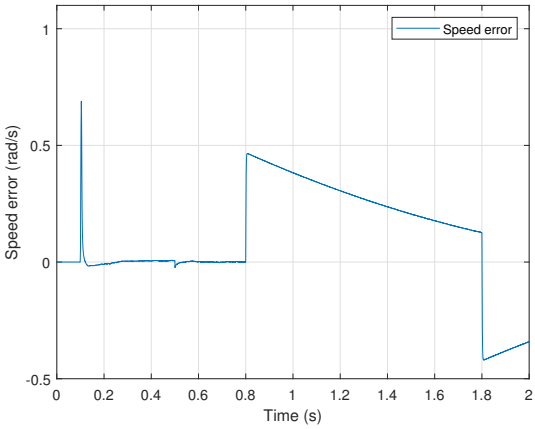

(d) Speed error: proposed DTC

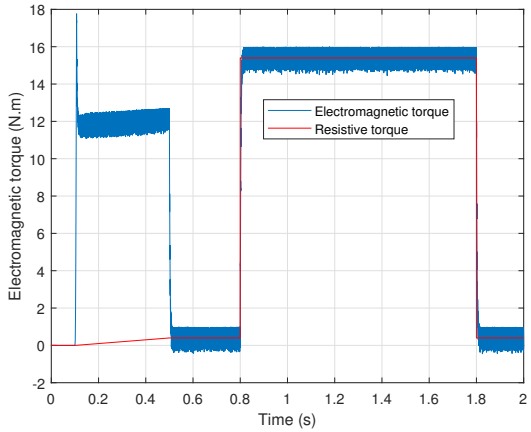

(e) Electromagnetic torque: conventional DTC

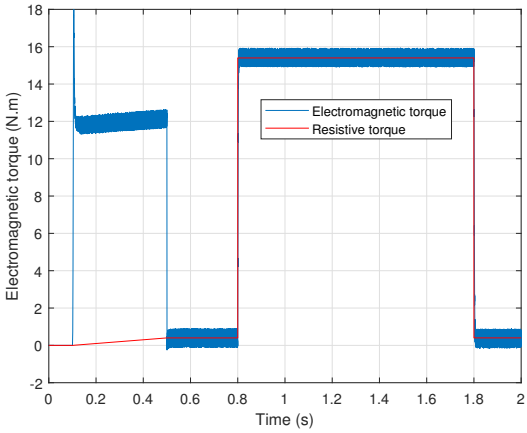

(f) Electromagnetic torque: proposed DTC

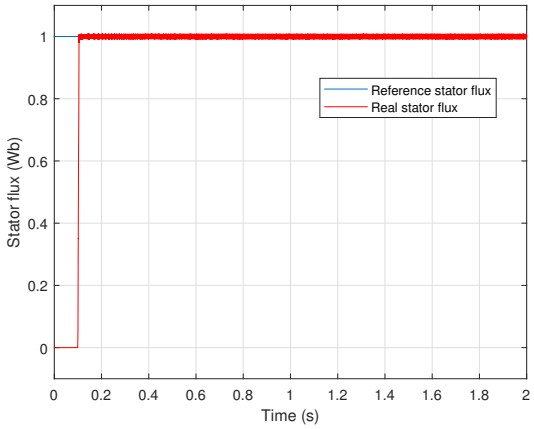

(g) Stator flux: conventional DTC

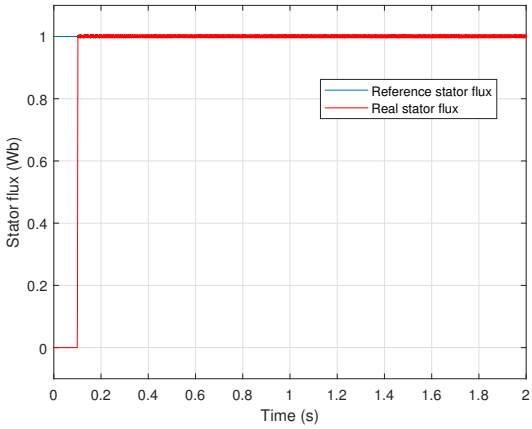

(h) Stator flux: proposed DTC

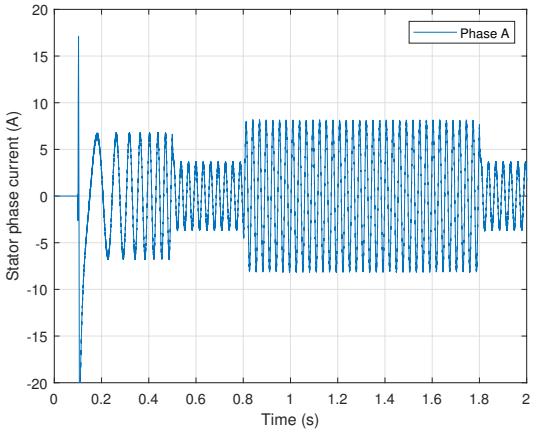

(i) Phase current: conventional DTC

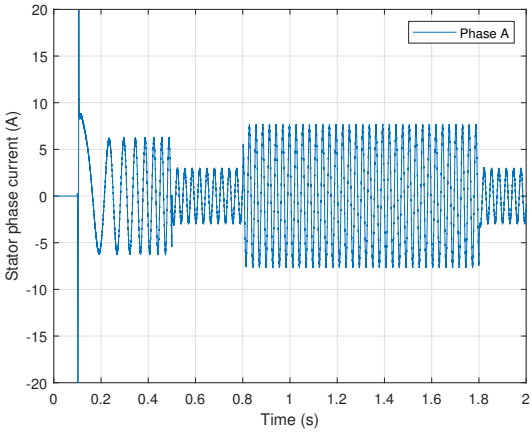

(j) Phase current: proposed DTC

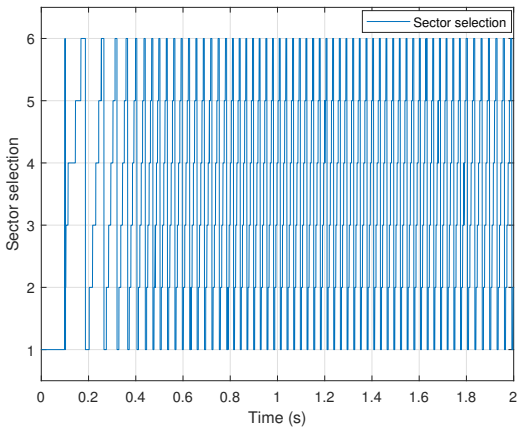

(k) Sector selection: conventional DTC

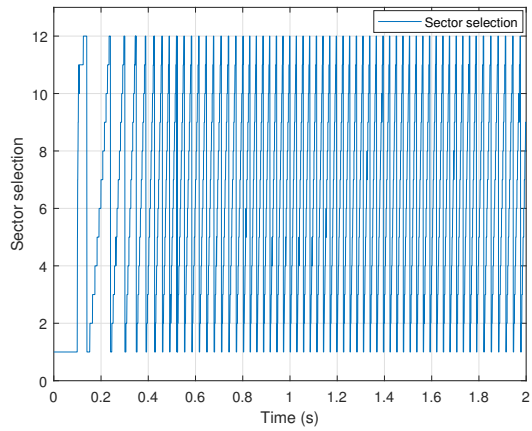

(l) Sector selection: proposed DTC

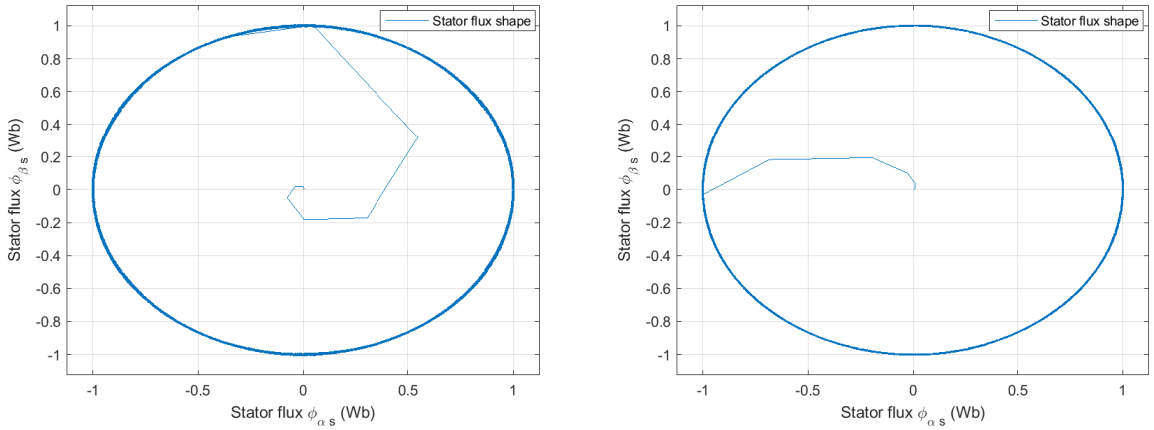

(m) Flux shape: basic DTC **(n)** Flux shape: suggested DTC

Fig. 7. Test under Ramp-Speed with Load Application

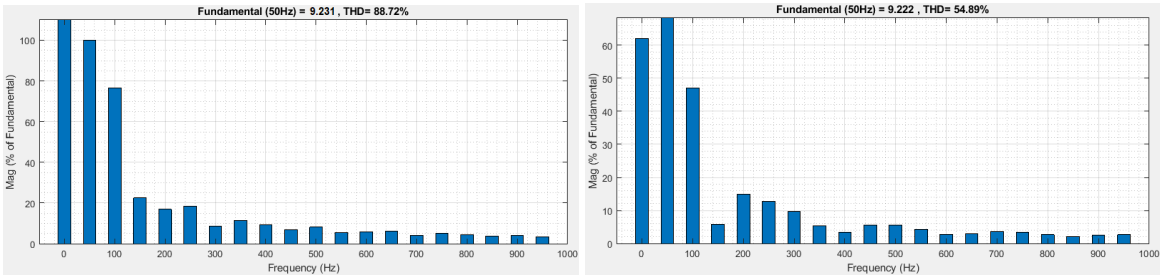

(a) Torque THD: basic DTC **(b)** Torque THD: suggested DTC

Fig. 8. Torque THD Improvement

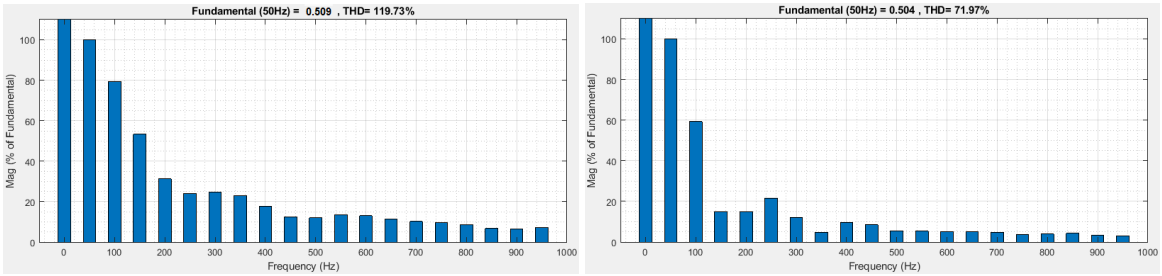

(a) Flux THD: basic DTC **(b)** Flux THD: suggested DTC

Fig. 9. Flux THD improvement

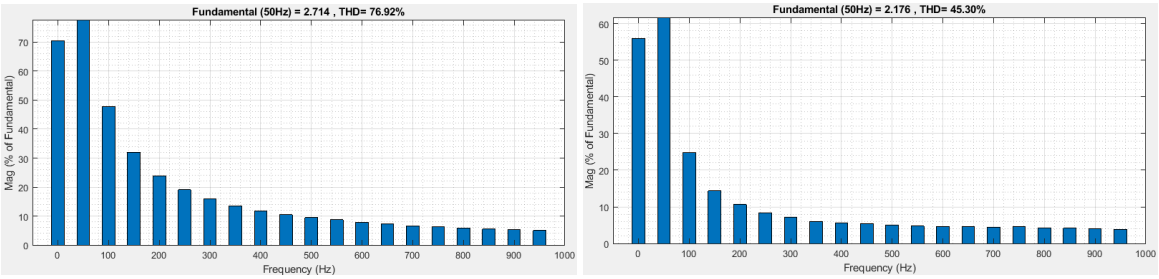

(a) Phase current THD: basic DTC **(b)** Phase current THD: suggested DTC

Fig. 10. Phase current THD improvement

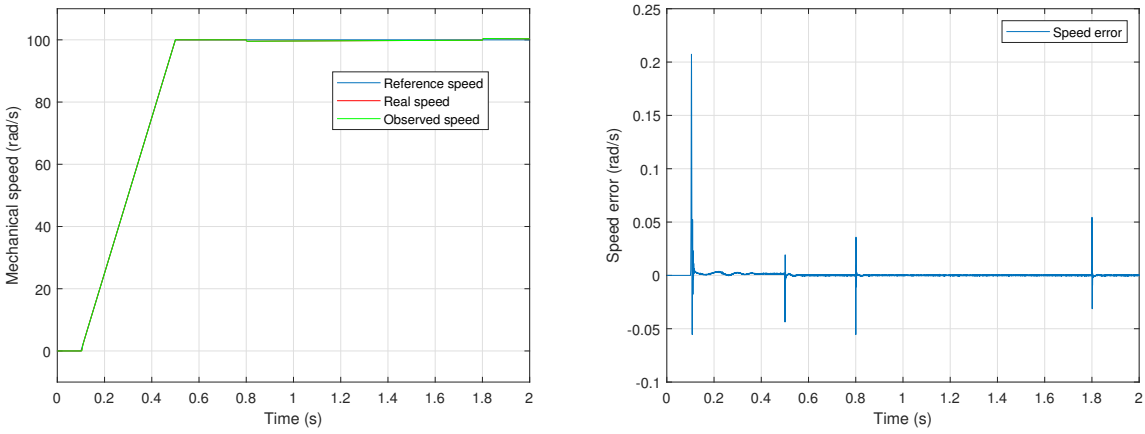

(a) Observed mechanical speed: suggested DTC **(b)** Speed observation error: suggested DTC

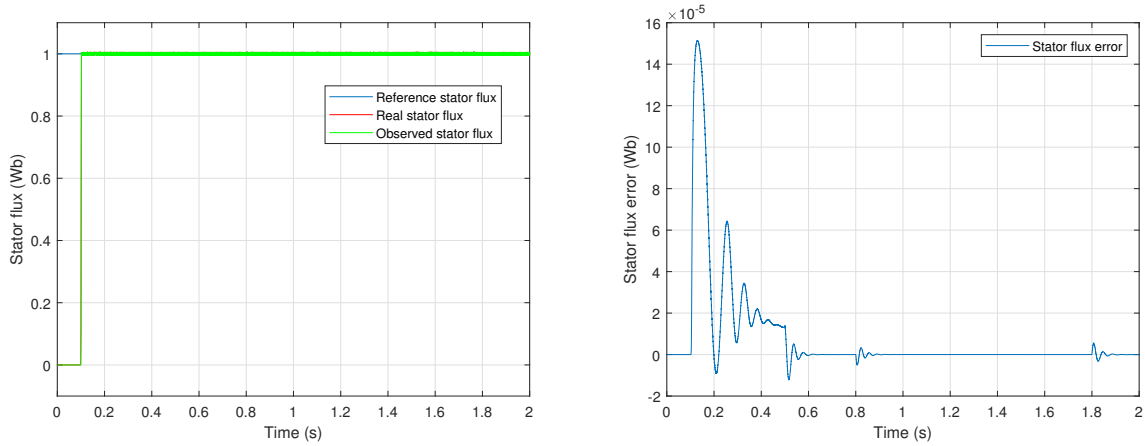

(c) Observed stator flux: suggested DTC **(d)** Flux observation error: suggested DTC

Fig. 11. Accuracy and precision of the fuzzy ALO observer

The basic DTC and the suggested iSTSMC-DTC show sinusoid waveforms in their stator current response. The current magnitude increased instantly directly after the load application. However, the basic DTC in Fig. 7(i) shows a chopped stator current waveform which indicates a high ripple level, while the proposed DTC in Fig. 7(j) shows a smoother waveform. This is justified in Fig. 10(b) where the suggested iSTSMC-DTC has a lower THD level (45.30%) compared to the conventional DTC (76.92%) in Fig. 9(a).

The evolution of the flux, such as its circular trajectory and magnitude, may be observed also. According to flux magnitude, the ripples surpass the hysteresis bands, which might be seen in Fig. 7(m). In addition, and because the zone changing, the flux takes initially a few steps before catching the referenced flux magnitude in Fig. 7(k). Also, the flux components show a fair waveform but a high ripple level. The suggested iSTSMC-DTC shows a decreased level of flux ripples, faster magnitude tracking at the start-up, and better components waveform compared to the conventional DTC. This is because the flux vector better zone selection in the suggested technique Fig. 7(l).

Highlights the sensorless control effectiveness show in Fig. 11. The speed margin between the real and the observed speed in Fig. 11(a) does not exceed 0.25 *rad/s* Fig. 11(b). And the flux margin between the observed and the real flux in Fig. 11(c) is very very little and does not exceed 16×10^{-5} *Wb* Fig. 11(d). The fuzzy adaptation mechanism in the adaptive Luenberger observer allows a perfect tracking of the real quantities with less static error. The choice of seven membership functions in the fuzzy algorithm allows a smooth choice of the suitable value to adjust the observed mechanical speed. The fuzzy ALO described in this research is an extended observer, it observes four state parameters and the mechanical speed. The four parameters are the motor state vector: $I_{s\alpha}$, $I_{s\beta}$, $\Phi_{s\alpha}$, and $\Phi_{s\beta}$.

7. Conclusion

This research suggested a twelve-sector DTC based on high-order SMC for induction motor performance improvement. The technique is built on the fundamental induction motor and two-level inverter equations. The suggested control is designed by mixing the integral sliding mode control and super-twisting algorithm, that not only solved the problem of chattering but also enhanced the global system stability and robustness. The Lyapunov theorem has been used to mathematically examine and demonstrate the system stability, and the twelve-sector iSTSMC-DTC command has been compared with the classical six-sector PI-DTC under load disturbance. The superiority of the suggested technique for disturbance rejection, overshoot, and load variations is shown by the simulation results. Besides, the suggested fuzzy ALO gave superior performance in closed-loop with the iSTSMC regulator. Basing on the obtained results in this research, it is clear that the principal ameliorations are:

- Elimination of natural chattering in basic SMC.
- The rotor speed quick response in the transient regime.
- The twelve-sector DTC based on iSTSMC with fuzzy ALO makes the system very accurate and faster.

Author Contribution: All authors contributed equally to the main contributor to this paper. All authors read and approved the final paper.

Funding: This research received no external funding.

Acknowledgment: The authors would like to thank the managers and the members of the "EIE laboratory" for their precious remarks and suggestions.

Conflicts of Interest: The authors declare no conflict of interest.

References

[1] A. Fathy Abouzeid, J. M. Guerrero, A. Endemaño, I. Muniategui, D. Ortega, I. Larrazabal, and F. Briz, "Control Strategies for Induction Motors in Railway Traction Applications," *Energies*, vol. 13, no. 3, p. 700, 2020, https://doi.org/10.3390/en13030700.

[2] Y. Zahraoui, M. Moutchou, S. Tayane, C. Fahassa, S. Elbadaoui, and A. Ma'arif, "Synchronous Reluctance Motor Performance Improvement Using MTPA Control Strategy and Five-Level Inverter Topology," *Journal of Robotics and Control (JRC)*, vol. 3, no. 5, pp. 725–734, 2022, https://doi.org/10.18196/jrc.v3i5.15326.

[3] Y. Azzoug, M. Sahraoui, R. Pusca, T. Ameid, R. Romary, and A. J. M. Cardoso, "High-performance vector control without AC phase current sensors for induction motor drives: Simulation and real-time implementation," *ISA Transactions*, vol. 109, pp. 295–306, 2021, https://doi.org/10.1016/j.isatra.2020.09.021.

[4] S. Mensou, A. Essadki, T. Nasser, B. B. Idrissi, and L. Ben Tarla, "Dspace DS1104 implementation of a robust nonlinear controller applied for DFIG driven by wind turbine," *Renewable Energy*, vol. 147, pp. 1759–1771, 2020, https://doi.org/10.1016/j.renene.2019.09.042.

[5] R. N. Mishra and K. B. Mohanty, "Development and implementation of induction motor drive using sliding-mode based simplified neuro-fuzzy control," *Engineering Applications of Artificial Intelligence*, vol. 91, p. 103593, 2020, https://doi.org/10.1016/j.engappai.2020.103593.

[6] A. Ammar, "Performance improvement of direct torque control for induction motor drive via fuzzy logic-feedback linearization: Simulation and experimental assessment," *COMPEL - The international journal for computation and mathematics in electrical and electronic engineering*, vol. 38, no. 2, pp. 672–692, 2019, https://doi.org/10.1108/COMPEL-04-2018-0183.

[7] S. Krim, S. Gdaim, A. Mtibaa, and M. Faouzi Mimouni, "FPGA-based real-time implementation of a direct torque control with second-order sliding mode control and input–output feedback linearisation for an induction motor drive," *IET Electric Power Applications*, vol. 14, no. 3, pp. 480–491, 2020, https://doi.org/10.1049/iet-epa.2018.5829.

[8] N. El Ouanjli, A. Derouich, A. El Ghzizal, S. Motahhir, A. Chebabhi, Y. El Mourabit, and M. Taoussi, "Modern improvement techniques of direct torque control for induction motor drives - a review," *Protection and Control of Modern Power Systems*, vol. 4, no. 1, p. 11, 2019, https://doi.org/10.1186/s41601-019-0125-5.

[9] M. Aktas, K. Awaili, M. Ehsani, and A. Arisoy, "Direct torque control versus indirect field-oriented control of induction motors for electric vehicle applications," *Engineering Science and Technology, an International Journal*, vol. 23, no. 5, pp. 1134–1143, 2020, https://doi.org/10.1016/j.jestch.2020.04.002.

[10] A. Saoudi, S. Krim, and M. F. Mimouni, "Enhanced Intelligent Closed Loop Direct Torque and Flux Control of Induction Motor for Standalone Photovoltaic Water Pumping System," *Energies*, vol. 14, no. 24, p. 8245, 2021, https://doi.org/10.3390/en14248245.

[11] E. W. Suseno and A. Ma'arif, "Tuning of PID Controller Parameters with Genetic Algorithm Method on DC Motor," *International Journal of Robotics and Control Systems*, vol. 1, no. 1, pp. 41–53, Feb. 2021. doi: https://doi.org/10.31763/ijrcs.v1i1.249.

[12] H. Dan, P. Zeng, W. Xiong, M. Wen, M. Su, and M. Rivera, "Model predictive control-based direct torque control for matrix converter-fed induction motor with reduced torque ripple," *CES Transactions on Electrical Machines and Systems*, vol. 5, no. 2, pp. 90–99, 2021, https://doi.org/10.30941/CESTEMS.2021.00012.

[13] V. Utkin, A. Poznyak, Y. Orlov, and A. Polyakov, "Conventional and high order sliding mode control," *Journal of the Franklin Institute*, vol. 357, no. 15, pp. 10 244–10 261, 2020, https://doi.org/10.1016/j.jfranklin.2020.06.018.

[14] C. Lascu, A. Argeseanu, and F. Blaabjerg, "Supertwisting Sliding-Mode Direct Torque and Flux Control of Induction Machine Drives," *IEEE Transactions on Power Electronics*, vol. 35, no. 5, pp. 5057–5065, 2020, https://doi.org/10.1109/TPEL.2019.2944124.

[15] H. Wang, Y. Yang, D. Chen, X. Ge, S. Li, and Y. Zuo, "Speed-Sensorless Control of Induction Motors With an Open-Loop Synchronization Method," *IEEE Journal of Emerging and Selected Topics in Power Electronics*, vol. 10, no. 2, pp. 1963–1977, 2022, https://doi.org/10.1109/JESTPE.2021.3050805.

[16] M. Morawiec, P. Kroplewski, and C. Odeh, "Nonadaptive Rotor Speed Estimation of Induction Machine in an Adaptive Full-Order Observer," *IEEE Transactions on Industrial Electronics*, vol. 69, no. 3, pp. 2333–2344, 2022, https://doi.org/10.1109/TIE.2021.3066919.

[17] E. Zhao, J. Yu, J. Liu, and Y. Ma, "Neuroadaptive dynamic surface control for induction motors stochastic system based on reduced-order observer," *ISA Transactions*, vol. 128, pp. 318–328, 2022, https://doi.org/10.1016/j.isatra.2021.09.006.

[18] N. El Ouanjli, S. Mahfoud, M. S. Bhaskar, S. El Daoudi, A. Derouich, and M. El Mahfoud, "A new intelligent adaptation mechanism of MRAS based on a genetic algorithm applied to speed sensorless direct torque control for induction motor," *International Journal of Dynamics and Control*, vol. 10, no. 6, pp. 2095–2110, 2022, https://doi.org/10.1007/s40435-022-00947-z.

[19] R. Yildiz, M. Barut, and E. Zerdali, "A Comprehensive Comparison of Extended and Unscented Kalman Filters for Speed-Sensorless Control Applications of Induction Motors," *IEEE Transactions on Industrial Informatics*, vol. 16, no. 10, pp. 6423–6432, 2020, https://doi.org/10.1109/TII.2020.2964876.

[20] T. Pham Van, D. Vo Tien, Z. Leonowicz, M. Jasinski, T. Sikorski, and P. Chakrabarti, "Online Rotor and Stator Resistance Estimation Based on Artificial Neural Network Applied in Sensorless Induction Motor Drive," *Energies*, vol. 13, no. 18, p. 4946, 2020, https://doi.org/10.3390/en13184946.

[21] Z. Boulghasoul, Z. Kandoussi, A. Elbacha, and A. Tajer, "Fuzzy Improvement on Luenberger Observer Based Induction Motor Parameters Estimation for High Performances Sensorless Drive," *Journal of Electrical Engineering & Technology*, vol. 15, no. 5, pp. 2179–2197, 2020, https://doi.org/10.1007/s42835-020-00495-6.

[22] I. Sami, S. Ullah, A. Basit, N. Ullah, and J.-S. Ro, "Integral Super Twisting Sliding Mode Based Sensorless Predictive Torque Control of Induction Motor," *IEEE Access*, vol. 8, pp. 186 740–186 755, 2020, https://doi.org/10.1109/ACCESS.2020.3028845.

[23] X. Yu, Y. Feng, and Z. Man, "Terminal Sliding Mode Control – An Overview," *IEEE Open Journal of the Industrial Electronics Society*, vol. 2, pp. 36–52, 2021, https://doi.org/10.1109/OJIES.2020.3040412.

[24] S. Jnayah and A. Khedher, "DTC of Induction Motor Drives Fed By Two and Three-Level Inverter: Modeling and Simulation," in *2019 19th International Conference on Sciences and Techniques of Automatic Control and Computer Engineering(STA)*, pp.376–381, 2019, https:doi.org/10.1109/STA.2019.8717227.

[25] X. Wu, W. Huang, X. Lin, W. Jiang, Y. Zhao, and S. Zhu, "Direct Torque Control for Induction Motors Based on Minimum Voltage Vector Error," *IEEE Transactions on Industrial Electronics*, vol. 68, no. 5, pp. 3794–3804, 2021, https://doi.org/10.1109/TIE.2020.2987283.

[26] Y. Zahraoui, M. Akherraz, and S. Elbadaoui, "Fuzzy Logic Speed Control and Adaptation Mechanism-Based Twelve Sectors DTC to Improve the Performance of a Sensorless Induction Motor Drive," *International Journal on Electrical Engineering and Informatics*, vol. 13, pp. 508–529, 2021, https://doi.org/10.15676/ijeei.2021.13.3.1.

[27] C. Fahassa, Y. Zahraoui, M. Akherraz, M. Kharrich, E. E. Elattar, and S. Kamel, "Induction Motor DTC Performance Improvement by Inserting Fuzzy Logic Controllers and Twelve-Sector Neural Network Switching Table," *Mathematics*, vol. 10, no. 9, p. 1357, 2022, https://doi.org/10.3390/math10091357.

[28] M. M. Alshbib, I. M. Alsofyani, and M. M. Elgbaily, "Enhancement and Performance Analysis for Modified 12 Sector-Based Direct Torque Control of AC Motors: Experimental Validation," *Electronics*, vol. 12, no. 3, p. 549, Jan. 2023, https://doi.org/10.3390/electronics12030549.

[29] M. Errouha, S. Motahhir, and Q. Combe, "Twelve sectors DTC strategy of IM for PV water pumping system," *Materials Today: Proceedings*, vol. 51, pp. 2081–2090, Jan. 2022, https://doi.org/10.1016/j.matpr.2021.12.214.

[30] Y. Zahraoui, M. Akherraz, C. Fahassa, and S. Elbadaoui, "Induction Motor DTC Performance Improvement by Reducing Flux and Torque Ripples in Low Speed," *Journal of Robotics and Control (JRC)*, vol. 3, no. 1, pp. 93–100, Jan. 2022, https://doi.org/10.18196/jrc.v3i1.12550.

[31] S. Pradhan, A. K. Sahoo, and R. K. Jena, "Comparison of DTC and SVM - DTC of Induction motor drive for Electric Vehicle application," in *2022 International Conference on Intelligent Controller and Computing for Smart Power (ICICCSP)*, pp. 1–6, 2022, https://doi.org/10.1109/ICICCSP53532.2022.9862317.

[32] P. Gao, G. Zhang, and X. Lv, "Model-Free Hybrid Control with Intelligent Proportional Integral and Super-Twisting Sliding Mode Control of PMSM Drives," *Electronics*, vol. 9, no. 9, p. 1427, 2020, https://doi.org/10.3390/electronics9091427.

[33] S. Nassiri, M. Labbadi, and M. Cherkaoui, "Optimal Integral Super-Twisting Sliding-Mode Control for high efficiency of Pumping Systems," *IFAC-PapersOnLine*, vol. 55, no. 12, pp. 234–239, 2022, https://doi.org/10.1016/j.ifacol.2022.07.317.

[34] B. Kelkoul and A. Boumediene, "Stability analysis and study between classical sliding mode control (SMC) and super twisting algorithm (STA) for doubly fed induction generator (DFIG) under wind turbine," *Energy*, vol. 214, p. 118871, 2021, https://doi.org/10.1016/j.energy.2020.118871.

[35] G. V. Hollweg, P. J. Dias de Oliveira Evald, D. M. C. Milbradt, R. V. Tambara, and H. A. Gründling, "Lyapunov stability analysis of discrete-time robust adaptive super-twisting sliding mode controller," *International Journal of Control*, vol. 96, no. 3, pp. 614–627, 2023, https://doi.org/10.1080/00207179.2021.2008508.

[36] M. Usama, Y.-O. Choi, and J. Kim, "Speed Sensorless Control based on Adaptive Luenberger Observer for IPMSM Drive," in *2021 IEEE 19th International Power Electronics and Motion Control Conference (PEMC)*, pp. 602–607, 2021, https://doi.org/10.1109/PEMC48073.2021.9432536.

[37] M. Adamczyk and T. Orlowska-Kowalska, "Self-Correcting Virtual Current Sensor Based on the Modified Luenberger Observer for Fault-Tolerant Induction Motor Drive," *Energies*, vol. 14, no. 20, p. 6767, 2021, https://doi.org/10.3390/en14206767.

[38] Z. Yin, C. Bai, N. Du, C. Du, and J. Liu, "Research on Internal Model Control of Induction Motors Based on Luenberger Disturbance Observer," *IEEE Transactions on Power Electronics*, vol. 36, no. 7, pp. 8155–8170, 2021, https://doi.org/10.1109/TPEL.2020.3048429.

[39] A. Boulmane, Y. Zidani, and D. Belkhayat, "Sensorless Vector Control of the IM Drives for an Urban Electric Vehicle Using Luenberger Observer with Fuzzy Adaptation Mechanism," in *2019 6th International Conference on Electrical and Electronics Engineering (ICEEE)*, pp. 28–32, 2019, https://doi.org/10.1109/ICEEE2019.2019.00013.

[40] Y. Azzoug, A. Menacer, T. Ameid, and A. Ammar, "Performance Improvement of Sensorless Vector Control for Induction Motor Drives using Fuzzy-Logic Luenberger Observer: Experimental Investigation," in *2019 International Conference on Applied Automation and Industrial Diagnostics (ICAAID)*, vol. 1, pp. 1–6, 2019, https://doi.org/10.1109/ICAAID.2019.8934966.